ELSEVIER

Journal of Chromatography A, 696 (1995) 1–18

JOURNAL OF CHROMATOGRAPHY A

NMR imaging of the chromatographic process Migration and separation of bands of gadolinium chelates

Ulrich Tallarek, Edgar Baumeister, Klaus Albert, Ernst Bayer, Georges Guiochon*

Institut für Organische Chemie, Universität Tübingen, Auf der Morgenstelle 18, D-72076 Tübingen, Germany

First received 27 September 1994; revised manuscript received 13 December 1994; accepted 14 December 1994

Abstract

The presence of gadolinium nuclei accelerates the relaxation of protons in their neighborhood. Using the imaging techniques of nuclear magnetic resonance developed for medical diagnosis, it is possible to observe the chromatographic bands of Gadolinium compounds which appear in shades of grey turning lighter with increasing gadolinium concentration. The existence of unexpectedly wide distributions of the local mobile phase velocity and the local height equivalent to a theoretical plate in an efficient chromatographic column is illustrated. The formation and resorption of fissured and/or compact zones in the column where the external porosity appears lower or higher than average is documented for the first time.

1. Introduction

Liquid chromatography is the most important method of laboratory-scale separations, whether for analytical or preparative purposes, because of the flexibility of this technique, the number of its applications and the variety of fields where it is encountered. Nevertheless, the structure of the column packing and the relationship between the column performance and this structure have been poorly studied and is still generally unknown. From a theoretical viewpoint, Giddings [1] drew the attention on the importance of the radial homogeneity of the column height equivalent to a theoretical plate (HETP) and the very harsh penalty in terms of efficiency loss caused by any long distance fluctuation of the local mobile phase velocity. Recently, Yun and Guiochon [2] have shown that considerable band spreading should arise in non-linear chromatography if even minor deviations from piston flow take place across the column and if the velocity at the column axis differs from the velocity at the column wall by a few percent.

Long ago, Knox and co-workers [3–5] studied the radial distribution of mobile phase flow velocity and local HETP in analytical columns. He showed that there are important, systematic variations. The mobile phase is somewhat faster along the column wall than in the axis, probably because dry packing causes a radial discrimination of the particles, with the larger falling closer to the wall. He also reported the existence of a region extending about 30 particle diameters from the wall, which is less homogeneous and exhibits a markedly lower efficiency. These re-

* Corresponding author. Present address: Department of Chemistry, University of Tennessee, Knoxville, TN 37996-1600, USA.

0021-9673/95/$09.50
SSDI 0021-9673(94)01231-8

sults were confirmed by Eon [6] who determined separately the axial and radial dispersion coefficients and showed that these parameters vary to a large extent across the column. The influence of bed homogeneity together with the problem of radial distribution of the sample at column inlet has been discussed by Skea [7] but without new experimental data. Recently, Baur et al. [8] and Farkas et al. [9] also obtained similar results confirming systematic variations of the flow velocity and local HETP across LC columns. However, using slurry-packed columns, they found the mobile phase velocity to be lower at the wall than in the center, by up to 8% [9], with a ridge of maximum velocity at about 2/3 of the radius from the center. The local HETP at the wall is nearly three times as high as that in the center. These results are in agreement with the conclusions of investigations of packed beds used as heat exchangers in chemical engineering [10,11], where the velocity of the stream is found to be significantly higher at the wall. They are also in agreement with observations which were made in preparative gas chromatography by Huyten et al. [12] and were explained theoretically and experimentally by Giddings and Fuller [13], documenting the particle size segregation in dry packing for the first time.

The problem has been generally ignored by the analytical community, as illustrated by the small number of relevant references. On the one hand, columns having reduced plate heights in the range between two and three are routinely produced and there is a widespread belief, albeit one unsupported by any fundamental or practical tenet, that 2 is a magic threshold and that it would not be possible to prepare columns with an HETP below twice the average particle diameter. As a matter of fact, values as low as 0.6 have been demonstrated by Knox and Parcher [3]. Furthermore, improvements on the performance of standard columns does not appear to be a high priority. On the other hand, there is no simple conceptual framework for the investigation of the structure of column packing and experimental studies require rather complex determinations of local concentrations which cannot be made using standard LC instrumentation. Previous measurements were made at the column exit, using electrochemical methods and very fine electrodes [3–6,8,9]. Using current techniques, it is difficult to acquire simultaneously measurements of the local concentrations of an analyte in a sufficiently large number of points of the column outlet cross-section to acquire the detailed representation needed of the distribution of the average residence times of the sample molecules in the column and of the variances of this distribution.

Although the importance of column homogeneity and packing density distribution appears to be minor in modern analytical HPLC, the problem is quite important in the preparative-scale applications of the method. This is essentially due to the much larger size of the column used, the possibility of large-scale fluctuations of the packing density which cause excessive losses in column performance, the direct relationship between column efficiency, recovery yield and cost, and the preeminent importance of economic considerations in the optimization of the process. However, if work is in progress on the assessment of the relationships between band profiles in non-linear chromatography and the velocity distribution inside the column [2,14], there are no data available on the distribution of packing density in large preparative columns, although the importance of achieving near plug flow has been stressed [7,15,16]. A discussion of the possible mechanisms through which non-plug flow could affect band profiles in the column and their warping or which could explain the injection of non-planar bands in a column [4,17] has been given by Skea [7]. The examination of colored bands immobilized inside columns after a certain time [15,18] provides information regarding only the band boundary and a few selected sections. It fails to provide a comprehensive picture of the band profile across the whole column. Other invasive approaches, such as the cutting of columns [19] or the insertion of thermocouples [20] has given only limited insights because of the very low spacial resolution of these techniques.

Clearly, progress in this area requires the use of more powerful investigative methods. The techniques developed for nuclear magnetic resonance imaging (NMR imaging, MRI) [21–23]

offer considerable potential for detailed investigations of local column properties [24] or for the monitoring in real time of the migration and dispersion of a band in a chromatographic column [25,26]. During the last decade, NMR imaging has become a powerful tool for medical diagnosis [27] and is now used also for non-medical imaging applications [28]. Combining the use of conventional NMR spectroscopy and of a magnetic field gradient this method yields images of any desired volume element or slide in a non-metallic object, be it a human body or the packing of a chromatographic column, provided the column tubing be non-metallic and a sufficient contrast can be achieved. In the present paper, we report on the use of a rapid imaging sequence (fast low-angle shot or FLASH) to monitor continuously the chromatographic separation of a mixture of gadolinium complexes. The same method permits the investigation of phenomena related to the introduction of the sample band inside the column.

We present here results obtained under non-satisfactory chromatographic conditions, in cases where the injection was not performed properly, the inlet filter was dirty, or the column inlet was damaged. This is more illustrative of the chromatographic process and of the possibilities to understand it better that are offered by the in situ, real-time imaging of the bands migrating along the column than results obtained under conditions of nominal performance [23]. The results reported here will clarify some of the reasons for the poor band profiles previously reported [22]. They should explain the importance of some aspects of chromatographic instrumentation which has been felt for a long time by chromatographers but have never been completely understood.

2. Theory of the method

2.1. Principle

The idea of using magnetic field gradient to enscribe in data obtained by NMR spectroscopy a code giving their location is nearly as old as NMR spectroscopy itself [29,30]. It is only in the 1970s, however, that Damadian [31], Lauterbur [32] and Mansfield and Grannell [33] independently showed how to operate space-resolved NMR spectroscopy. To the main, homogeneous, static magnetic field, $\boldsymbol{B}_0$, a much smaller, time-dependent linear gradient field, $\boldsymbol{G}(\boldsymbol{r},t)$, is superimposed. A proton resonates at the Larmor frequency and we have the following relationship between this frequency and the location [34–37]

$$\boldsymbol{B}(\boldsymbol{r},t) = \boldsymbol{B}_0 + \boldsymbol{G}(\boldsymbol{r},t) \tag{1a}$$

$$\omega(\boldsymbol{r},t) = \gamma\boldsymbol{B}(\boldsymbol{r},t) = \omega_0 + \gamma\boldsymbol{G}\boldsymbol{r} \tag{1b}$$

This last equation expresses the fundamental principle of NMR Imaging. It is illustrated in Fig. 1 in the case of a one-dimensional gradient, for the sake of simplicity [38]. $\boldsymbol{G}$ is the gradient of the pulsed gradient field, $\boldsymbol{G}(\boldsymbol{r},t)$, parallel to the main magnetic field [34] and γ is the gyromagnetic ratio, specific of the nuclei considered [$\gamma(^1\mathrm{H}) = 2.675 \cdot 10^8\ \mathrm{T}^{-1}\ \mathrm{s}^{-1}$]. $\boldsymbol{G}$ has for its components $G_x = \partial B_z/\partial x$, $G_y = \partial B_z/\partial y$ and $G_z = \partial B_z/\partial z$. As a consequence, the frequency spreads, hence the spatial resolution achieved are directly proportional to the pulse gradient strength and to the dimension of the object, with $\Delta\omega = \gamma\boldsymbol{G} \cdot \Delta\boldsymbol{r}$.

The goal in imaging methods is to derive from the signal acquired the distribution of the structural density of the object, $\rho(\boldsymbol{r})$. In NMR imaging this function is the local nuclear spin density. The basic imaging scheme is illustrated in Fig. 2 [39]. It is obvious from this figure that the signal, $S(\boldsymbol{k})$ where $\boldsymbol{k}$ is the reciprocal space vector, and the local spin density, $\rho(\boldsymbol{r})$, are related by Fourier transform and inverse Fourier transform. The concept of reciprocal space vector in MRI was introduced by Mansfield and Grannell [40,41]. It is related to the magnetic field gradient by

$$\boldsymbol{k} = (2\pi)^{-1}\gamma\boldsymbol{G}t \tag{2}$$

and

$$S(t) = \int\int\int(\boldsymbol{r})\ \exp\ (i\gamma\boldsymbol{G}\boldsymbol{r}t)\mathrm{d}\boldsymbol{r} \tag{3}$$

Thus, both $\boldsymbol{G}$ and t are involved in the study of the reciprocal space or $\boldsymbol{k}$ space. $\boldsymbol{G}$ determines also the direction that is followed in any move-

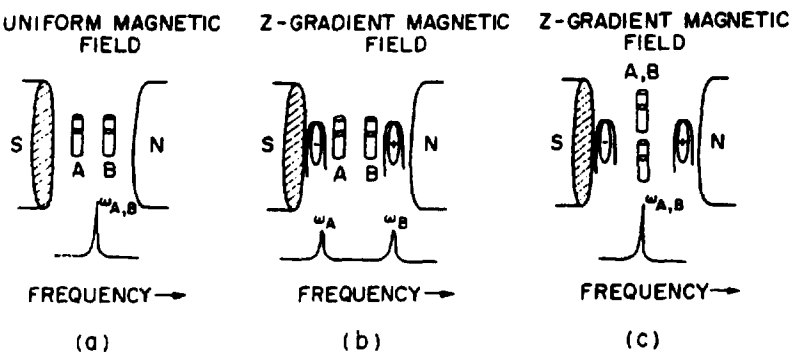

Fig. 1. Resonance frequencies of water in two capillaries placed in a magnetic field. (a) Uniform magnetic field, $\omega_A = \omega_B = \gamma B_0$. (b, c) Linear field gradient in the main field axis, $\omega_A = \gamma(B_0 + z_A G_z)$, $\omega_B = \gamma(B_0 + z_B G_z)$ and $\Delta\omega = \gamma(z_A - z_B)G_z$ [38]. The Fourier transform of the FID gives a one-dimensional projection of the integral spin density on a line parallel to the direction of the applied gradient.

ment through the k space. For reconstruction of the image, the k space is sampled systematically by varying the magnitude of the magnetic field gradient or by moving in time [37,42–44]. A Fourier transform is then performed on the data acquired. In practice, this is done by sampling the NMR signal [i.e., the free induction decay (FID) or an echo of the spins] in the time domain because the reciprocal space and the image space correspond to the time and frequency domains, respectively. By choosing the direction of the magnetic field gradient, it is possible to select the slice of the column which will be imaged.

2.2. Implementation

The visualization of the chromatographic process requires a contrast between the region of the column where the band is located and the upstream and downstream regions where the solute concentration is negligibly small. Several approaches are possible. For example, we could observe in ^{19}F NMR bands of bis-trifluorobenzene derivatives eluted in conventional reversed-phase chromatography [45]. The fluorine signal would give the required information. The converse approach, the elution of an alkyl derivative by a fluorinated solvent would be more difficult to implement, since it would require the use of a non-protonated adsorbent. The chemical shift of ^1H is insufficient to permit both the rejection of the signals for the uninteresting protons and a satisfactory signal/noise ratio. We decided for a different approach, permitting both the use of the ^1H NMR signal and of conventional chromatographic conditions. It is well known that the gadolinium ion, Gd^{3+}, considerably reduces the

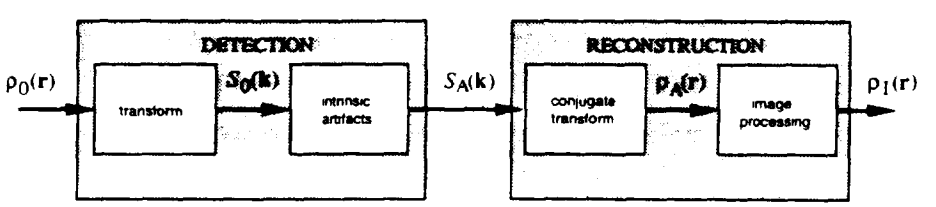

$$S(\mathbf{k}) = \iiint \rho(\mathbf{r}) \exp[i2\pi \mathbf{k}\cdot\mathbf{r}]\, d\mathbf{r} \qquad \rho(\mathbf{r}) = \iiint S(\mathbf{k}) \exp[-i2\pi \mathbf{k}\cdot\mathbf{r}]\, d\mathbf{k}$$

Fig. 2. Schematic representation of the imaging process [39].

relaxation times of the nearby protons. This ion has seven unshared electrons, is in the configuration f^7 ($\mu_{eff} = 8.0$ B.M. [46]), and gives strong electron–nucleus dipole–dipole interactions [47–51]. Thus, Gd^{3+} or its complexes can be visualized indirectly by the relaxation time differences of the mobile phase protons which they induce locally. One advantage of the approach is that it is possible to find different Gd^{3+} chelates which can be separated by chromatography and yet their response factors will be the same, allowing for the direct use of relative response in our investigations.

3. Experimental

3.1. Liquid chromatography

A Merck (Darmstadt, Germany) Superformance glass column (2.6 cm I.D. × total length 50 cm with fittings and connecting tubes, bed length, 15 cm) was used. The column was packed with LiChrospher RP-18 (Merck), 15 μm average particle size. The bed packing was achieved by permitting a concentrated slurry of the adsorbent to settle in the column over a period of several days. The actual bed length was only 13.5 cm. The system was completed by a SYKAM S 1100 pump (Gilching, Germany), a Rheodyne sampling valve (Cotati, CA, USA) and a Linear UVIS 204 detector (Reno, NV, USA). These devices were connected to the column by plastic tubing since the amount of non-magnetic metal brought inside the scanner must be small and located as far from the column as possible, not to perturb the image. Because the pump and the sampling valve are weakly magnetic, they have to be placed far enough from the column, at ca. 1.5 m. A 0.8 mm I.D. PTFE tubing was used for the connection. This causes a significant extra-column contribution to band broadening. The mobile phase was a buffer solution (see below). Neither the water used nor the buffer solution were filtered before use, contrary to standard analytical practice, which explains some of the illustrative results.

Chromatograms obtained under (i) conventional analytical conditions (connecting tubes having the same diameter but 30 cm long) before the beginning of the imaging experiments, (ii) after the second series of imaging experiments and (iii) after repair of the column, respectively, are shown in Fig. 3. They illustrate the variation in performance and should be compared to the images of the band discussed later. Note that the reduced HETP of the last peak of the chromatogram, *n*-butylbenzene, is 2.1, a value which is usually considered to be very good, in Fig. 3a, 12.0 in Fig. 3b, and 5.1 in Fig. 3c.

3.2. NMR system

The column was first placed inside an 8 cm I.D. solenoid coil (transmitter/receiver coil length, 10 cm) and this assembly was positioned horizontally in the middle of the superconducting whole body imager (Magnetom 63; Siemens, Erlangen, Germany) of the University of Tübingen. This imager operates at 1.5 T, corresponding to a frequency of approximately 63.6 MHz for proton imaging. The gradient system consists of three mutually orthogonal coil groups that can produce any desired gradient, in any direction respective to the axis of the main magnetic field. The entire system is schematized in Fig. 4. The maximum gradient strength is 9.6 mT/m. The column and the solenoid which surrounds it are positioned orthogonal to the tunnel axis, i.e., to the direction of the main magnetic field. The system permits the acquisition of images of the concentration distribution of the gadolinium concentration in any planar direction. For example, it is possible to scan slices and measure the distribution of Gd concentration in any section of the column parallel or perpendicular to its axis. The direction of this plane is chosen by setting the magnetic field gradient in the appropriate direction. The image can be updated every 7 s. In most cases (and unless stated otherwise in the figure caption), the image of the column cross-section (26 × 135 mm) is included in a 166 × 166 mm field of view, given as a 256 × 256 matrix Thus, the individual pixel corresponds to a rectangle of column packing having 0.65 × 0.61 mm. In the construction of the image, the signal is averaged over a thickness of ca 1 mm.

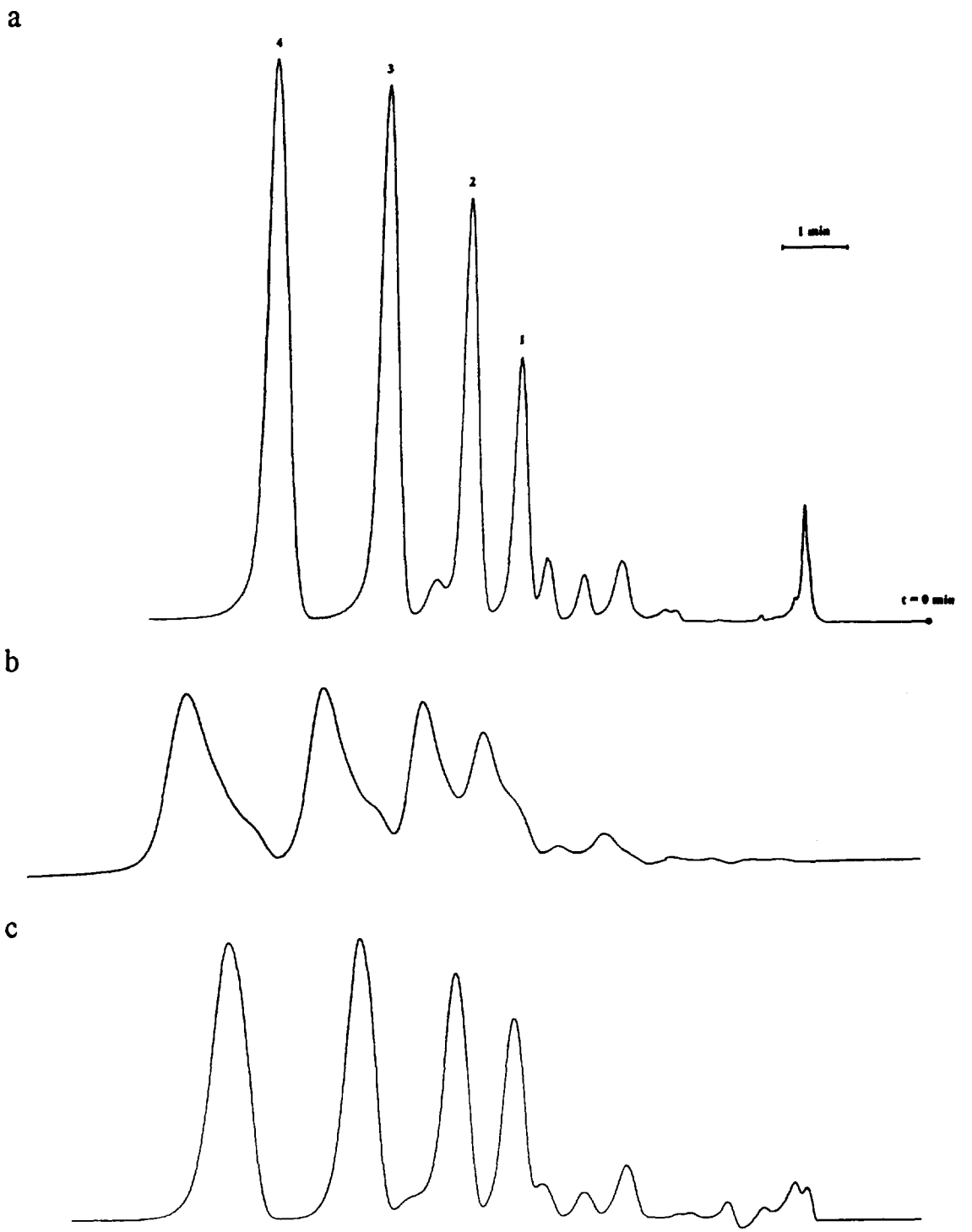

Fig. 3. Chromatogram of a test mixture. Peaks: 1 = toluene; 2 = ethylbenzene; 3 = *n*-propylbenzene; 4 = *n*-butylbenzene. (a) Beginning of the imaging experiments; (b) after the second series of imaging experiments (i.e., between Figs. 18 and 19); (c) after repair of the column. Mobile phase, water–acetonitrile (15:85), 6 ml/min, UV detection at 254 nm.

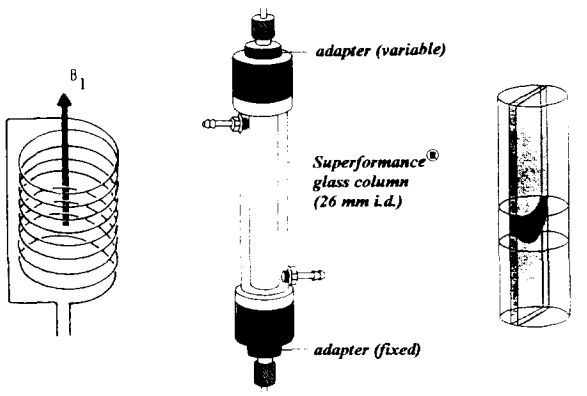

Fig. 4. Schematic representation of the imaging of a band in the chromatographic column. Left, transmitter/receiver solenoid inside which is located the column. Center, preparative glass column. Right, schematic illustration of the concentration distribution of the gadolinium complex in an axial slice of the column bed selected by an appropriate choice of the magnetic field gradient.

One of the difficulties of the experiment is the non-linear behavior of the signal which is not proportional to the gadolinium concentration. A calibration curve of ^{57}Gd in pure water is shown in Fig. 5 [52]. Above a certain concentration (approximately 1 mM), the response decreases with increasing concentration and beyond about 6 mM, it is lower than with no gadolinium. As a consequence, the regions where there is no gadolinium appear dark grey. Certain regions of the column may appear black because the local concentration of gadolinium is too high. This situation is avoided as much as possible by using small samples.

3.3. Choice of the analytes

The signal intensity of the pixels of the images obtained for different column slices depend on the spin-lattice relaxation times, T_1, and the spin–spin relaxation times, T_2, the spin density, the flow velocity, the intensity of some diffusion phenomena and the chemical shift of the nuclei present [53]. Local differences between the values of these parameters cause image contrast under selected conditions. Arranging for the proper contrast permits the acquisition of certain selected information. The visualization of a chromatographic separation requires the use of a soluble, stable compound.

Gadolinium gives stable complexes of Gd^{3+} with various organic ligands [54,55]. These chelates were used for the visualization of the chromatographic process as explained in a previous section. They were separated by reversed-phase ion-pair chromatography, a mode which permits an easy selection of experimental conditions allowing suitable retention of these chelates as anions [56]. The mobile phase was a

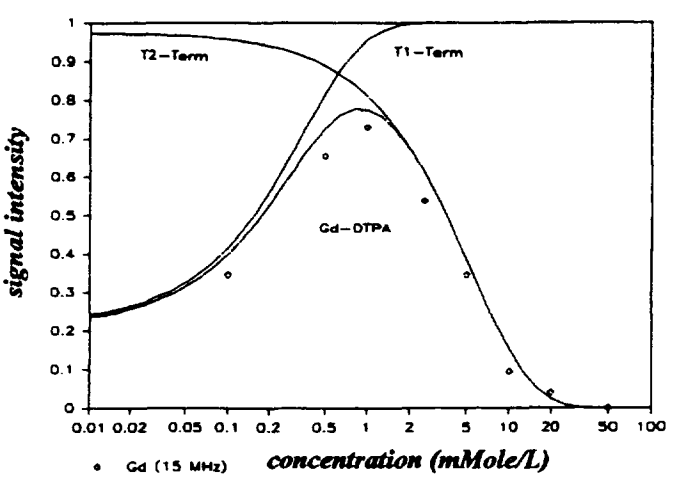

Fig. 5. Calibration curve. Plot of the signal observed versus the concentration in Gadolinium. Solid line, calculated response. Symbols, experimental data.

solution of water and acetonitrile (85:15), containing 5 m*M* KH_2PO_4 and 4 m*M* *n*-octylamine, at a pH of 5. Chelates of ethylenediaminetetraacetic acid (EDTA), *trans*-1,2-cyclohexanediaminetetraacetic acid (CDTA), ethyleneglycolbis(aminoethyl)tetraacetic acid (EGTA) and diethylenetriaminepentaacetic acid (DTPA) were prepared following classical procedures. Their structures are shown in Fig. 6. At pH 5, these complexes are completely deprotonated [57–59] and exist in solution as the anions $Gd(EDTA)^-$, $Gd(CDTA)^-$, $Gd(EGTA)^-$ and $Gd(DTPA)^{2-}$, respectively.

Saturated solutions of the complexes were freshly prepared and filtered before use. They were mixed and diluted to the proper concentration immediately prior to the experiments.

4. Results and discussion

Fig. 7 is an attempt to represent a three-dimensional image of a chelate band [60]. It shows a series of images giving the distribution of Gd concentration in 26 horizontal planes equally spaced. The distance between two successive such planes is approximately 1 mm. The images 1 and 26 correspond approximately to the planes tangent to the top and bottom of the column. Images 13 and 14 are 0.5 mm above and below the column axis, respectively. The combination of these images permits a reconstitution of the three-dimensional concentration distribution in the band at a migration distance of approximately 45 mm (see Fig. 4). These images were obtained with a rapid imaging sequence

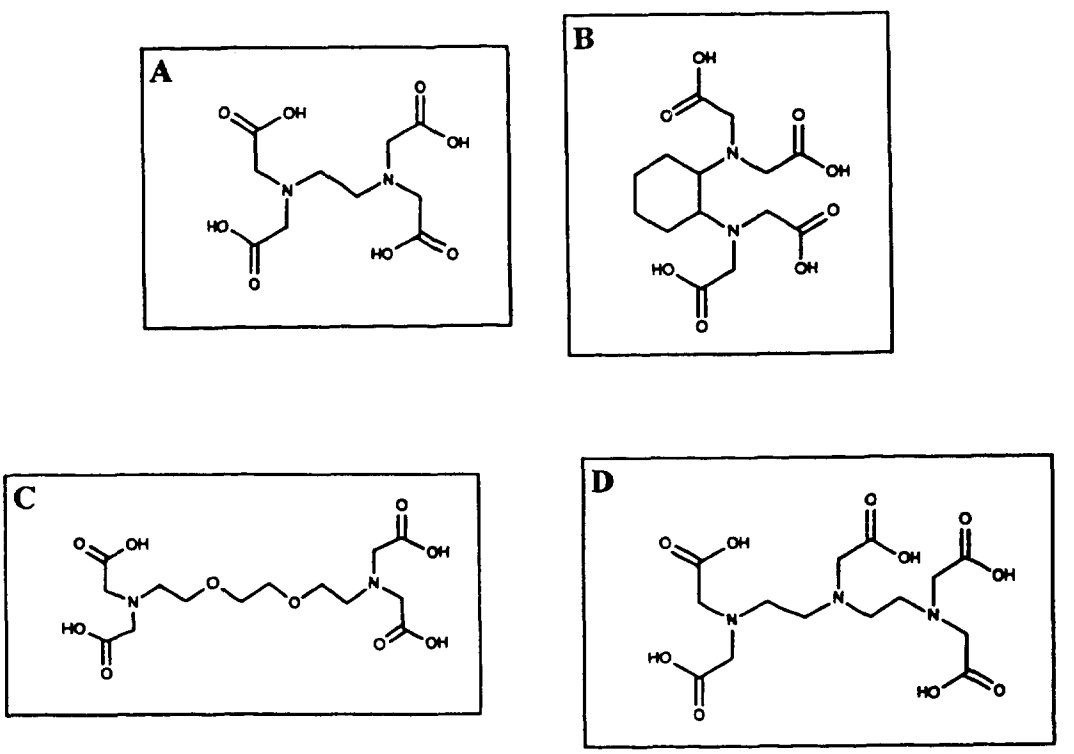

Fig. 6. Structures of the organic ligands of the gadolinium chelates used. (A) Ethylenediaminetetraacetic acid (EDTA); (B) *trans*-1,2-cyclohexanediaminetetraacetic acid (CDTA); (C) ethyleneglycolbis(aminoethyl)tetraacetic acid (EGTA); (D) diethylenetriaminepentaacetic acid (DTPA).

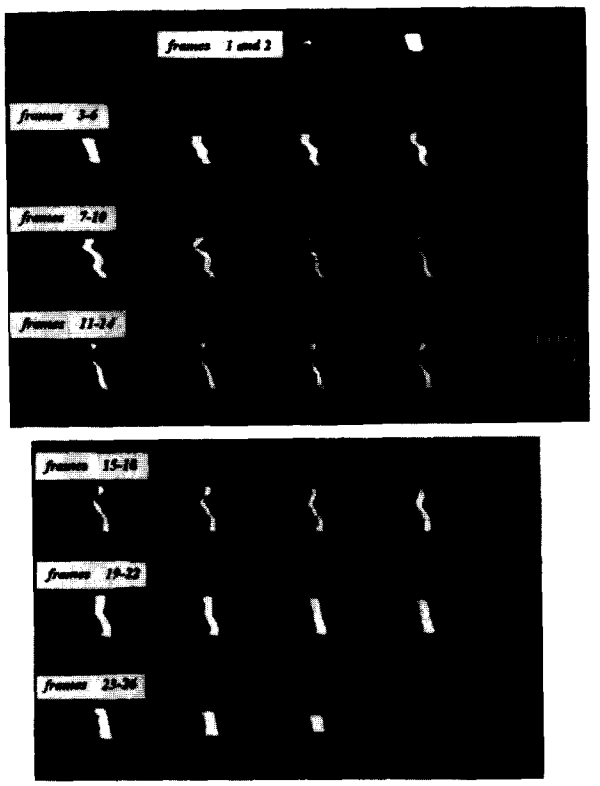

Fig. 7. Series of three-dimensional FLASH images [50] of a band of Gd(DTPA) in the chromatographic column. These images give the three-dimensional distribution of Gd concentration at a given time, corresponding to a migration distance of approximately 45 mm. Flip angle (FA), 90°; repetition time (T_R), 0.04 s; echo time (T_E), 10 ms; slice thickness (SL), 1 mm; matrix size, 128 × 128; flow from left to right. The 26 images correspond to the concentration distribution in as many sections of the column by horizontal planes (i.e., parallel to the column axis).

(FLASH [61,62]), using short repetition times (0.04 s). This procedure gives signals only for protons which have relaxed sufficiently during the repetition time, i.e., those which are in the vicinity of Gd atoms: the relaxation rate enhancement is proportional to R^{-6}, with R distance between Gd and proton. Thus, the chelates are indirectly visualized as bright zones (T_1 contrast).

We note in Fig. 7 that the pattern of the concentration distribution is far from uniform. Since injection was done with a sampling valve, its front should be flat. The important deviations from a planar distribution observed in images 6–19 suggest a strong gradient of migration velocity across the column. This, in turn, can be explained by a non-homogeneous distribution of the retention factors or of the mobile phase velocity (or both). The latter is the more important, as local fluctuations of the packing density of the column result in larger fluctuations of the local external column porosity, hence much larger fluctuations of the flow velocity, than of the retention factor. The retention factor is proportional to the local density of stationary phase, $(1-\epsilon_e)\rho_a$, where ϵ_e is the external porosity (ratio of the volume available to the mobile phase stream around the particles to the geometrical volume of the column, of the order of 0.35 to 0.40) and ρ_a is the apparent density of the particles of adsorbent. A fluctuation of packing density resulting in a relative change of the porosity $\Delta\epsilon_e/\epsilon_e$ will cause a relative change in

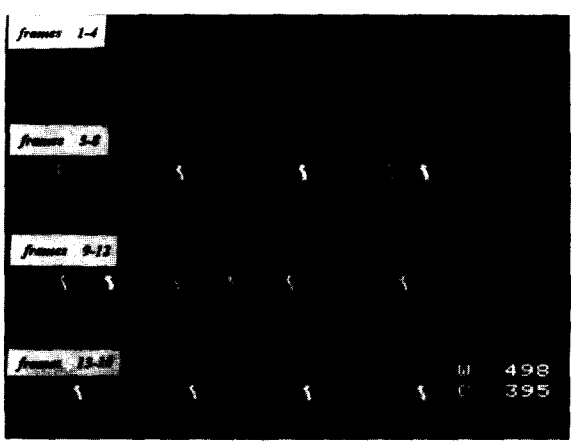

Fig. 8. Two-dimensional FLASH images from the separation of bands of Gd(EGTA) and Gd(DTPA). These images were taken at different times and are all cross-section of the concentration distribution by the horizontal plane through the column axis. Flow-rate, 6 ml/min, from left to right. Same experimental conditions as in Fig. 7, except $T_R = 0.03$ s, SL = 4 mm and matrix size, 256 × 256.

the local retention factor nearly 1.6 times lower (value of the ratio $(1-\epsilon_e)/\epsilon_e$) and, because of the Blake–Kozeny equation relating the external porosity and the permeability, a relative change in the permeability 4.5 time larger, hence a 7 times larger effect on the flow velocity than on the retention time.

Indeed, the band profile does not correspond to what would be expected under plug flow conditions and could be interpreted as suggesting an important variation of the permeability in the radial direction. We note, however, that the distribution is not cylindrical, nor even symmetrical as reported by previous workers [3–6,8,9] and expected for a cylindrical column packed by sedimentation. A careful examination of Figs. 8 and 9 shows that the velocity is nearly the same everywhere and that the profiles propagate nearly unchanged, except for some axial spreading (apparent axial dispersion [24]). These observations suggest an alternate explanation, the obstruction of the inlet filter of a region of the packing at the column inlet, interfering with the introduction of the band into the column without causing differential migration of parts of the profile. This possibility will be further discussed later.

The planar section of the three-dimensional band profiles shown in Fig. 7 were obtained all at the same time for a single component band [Gd(DTPA)]. Fig. 8 shows sections of the band profiles of Gd(EGTA) and Gd(DTPA) during their progressive separation by an horizontal plane through the column axis at different times. Gd(EGTA) is eluted first [26]. The first four frames in this figure are shown enlarged in Fig. 9. Comparison with frame 13 in Fig. 7 shows that the flow velocity distribution in the column has not changed much in the mean time. Note that the Gd(EGTA) band disappears after frame 10 because the resolution becomes too large to keep it in the figure. In Fig. 10, we show the con-

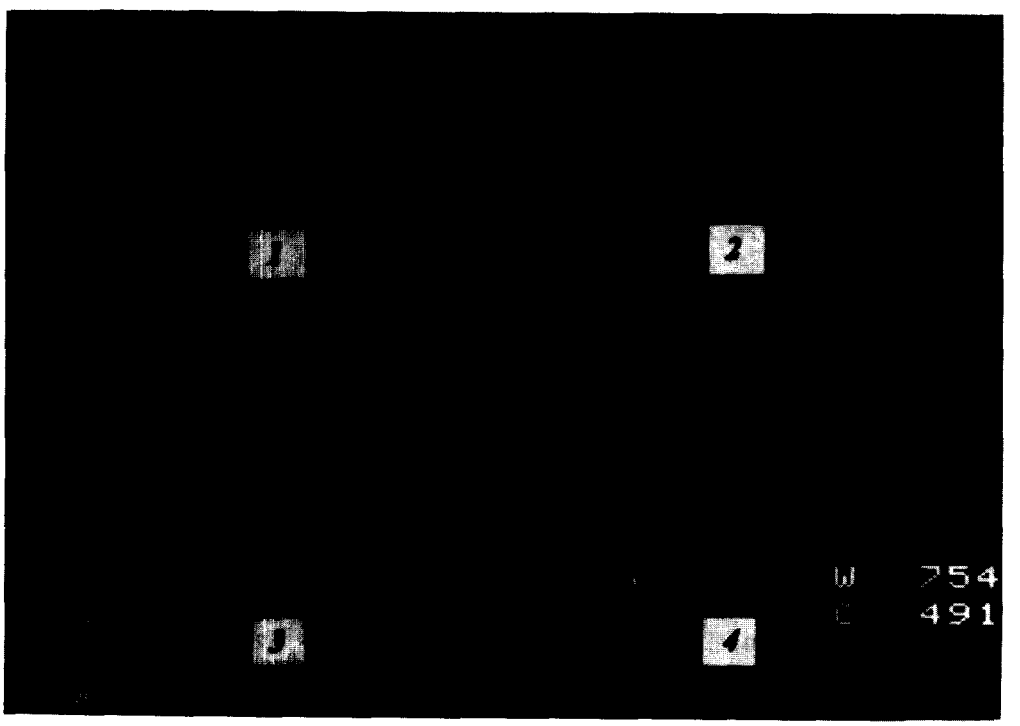

Fig. 9. Two-dimensional FLASH images of the progressive separation of bands of Gd(EGTA) and Gd(DTPA). Enlargement of the first four images in Fig. 8.

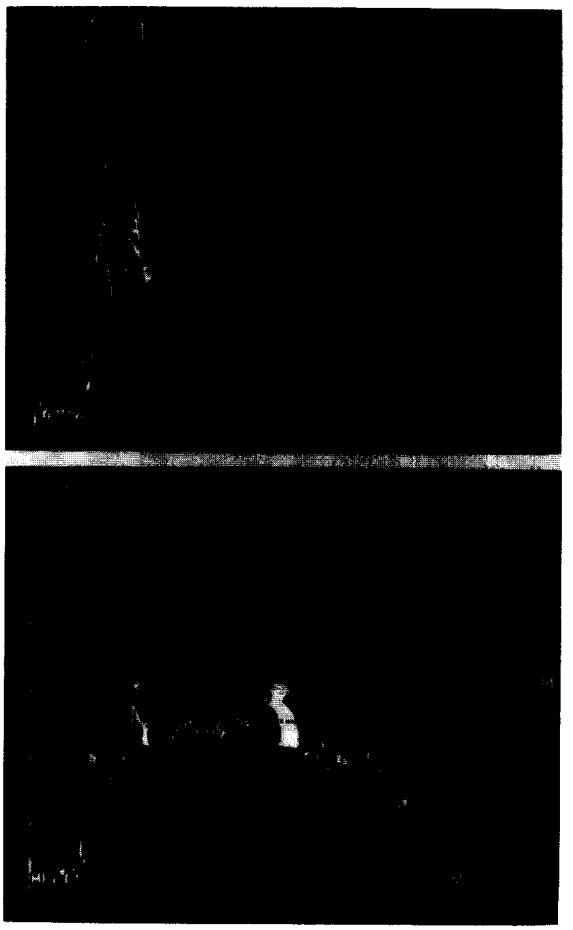

Fig. 10. Signal intensity profiles of the two bands of gadolinium complexes in Fig. 8 (frame 8) along the column axis.

centration profile along a parallel to the column axis for frame 8. The profiles are narrow and nearly symmetrical. Fig. 11 shows the two-dimensional planar section of the band profiles of Gd(EGTA), Gd(CDTA) and Gd(DTPA), eluted in this order [26]. The time evolved between frames 1 and 16 is approximately 2.8 min. The band profiles obtained are very similar to those shown above and to illustrations of the difficulties associated with separations of closely eluted bands when the plug flow condition is not satisfied (e.g., Ref. [7], Fig. 12.15). Note that while the column efficiency corresponded to a value of

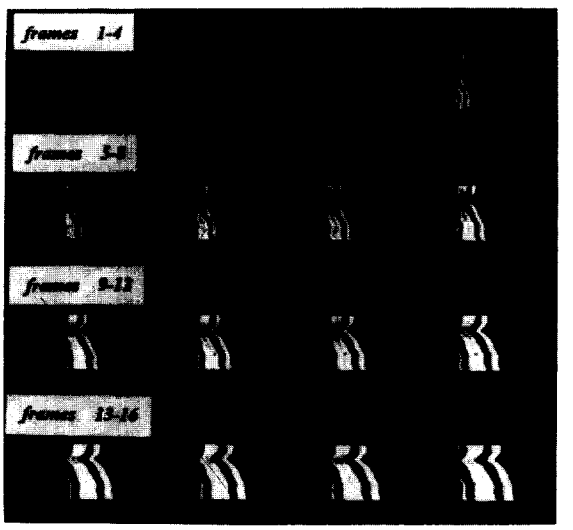

Fig. 11. Two-dimensional FLASH images of the bands of Gd(EGTA), Gd(CDTA) and Gd(DTPA) during their separation. Same conditions as for Fig. 8.

the reduced plate height of 2.1 at the beginning of the experiments (Fig. 3a), the efficiency calculated from the width of the zone in the direction parallel to its axis corresponds to a reduced plate height of 1.0 to 1.2, even though the column is connected to the injection valve through a 150 cm long tubing. The three bands in Fig. 11 are clearly well resolved in frame 6; they are most probably separated earlier. However, because the column is longer than the solenoid coil, the images of its ends are somewhat darker, obscuring the early separation. Obviously, the resolution achieved in frame 16 will be seriously degraded upon elution of the band system, the part of the bands along the right wall eluting earlier than the part along the left one.

The question then arises, what causes the band profile to assume a Λ-shape in the radial direction (Fig. 7, frames 9–17 and Figs. 8 to 11)? Figs. 12 and 13 demonstrate an increase in the extent of the band spreading or apparent axial dispersion for both Gd(EGTA) and Gd(DTPA) after one day of operation. In the same time, the permeability of the column decreases, forcing a reduction in the flow-rate used for the experi-

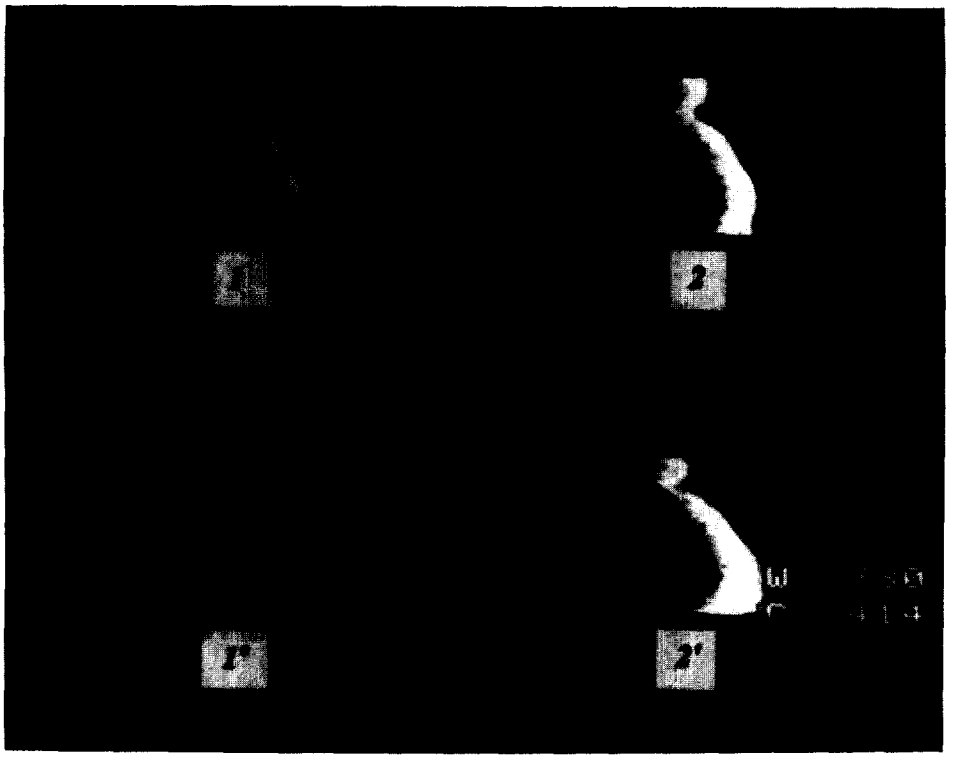

Fig. 12. Aging of a column. Comparison of the two-dimensional FLASH images of the bands of Gd(EGTA) and Gd(DTPA) after 5 min (1, 1') and of the bands of Gd (DTPA) after 30 min (2, 2') obtained at one day interval. Same selected slice, same NMR conditions as in Fig. 8, same time interval after injection. Flow-rate, 4 ml/min, left to right.

ments (from 6 to 4 ml/min). Progressive obstruction of the column inlet takes place. To investigate the origin and mechanism of this phenomenon, horizontal spin echo images of the column inlet were taken as well as FLASH images of its inlet, using a three-dimensional spin echo sequence [37]. They are presented in Fig. 14.

Fig. 14a shows sections of the column by several horizontal planes, below the column axis (frames 1 and 2), through the column axis (frame 3) and above this axis (frame 4). They all reveal a dark zone at the beginning of the column, much darker than observed normally. This result is explained by the presence of a significant amount of a metal which, like gadolinium, enhances the spin relaxation of ^{1}H. The amount is so large that no signal is observed under normal imaging conditions (this is known as the T_2 effect). The concentration of the deposits has to decay very sharply along the column, otherwise there would be a bright white band turning to grey just after the black band, see Fig. 5). Fig. 14b shows sections of the column by planes perpendicular to its axis and equidistant by about 2 mm. The first section is at the column inlet (i.e., in the filter, frame 1). They show that the column plugging is not homogeneous (frames 2–4). A dark spot is noticed off center in frame 2. Its position shows that it corresponds to the origin of the band perturbation (Figs. 7–13) and demonstrates that this perturbation took place at injection.

The direction of flow was then reversed in the column, which is against recommended laboratory practice in chromatography. The first injection, after the column has been flushed for about 15 min, gave the images in Figs. 15 and 16. Note that the flow direction being reversed, it now

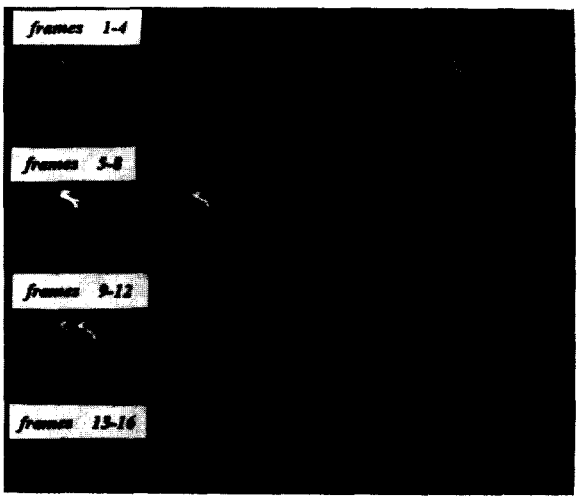

Fig. 13. Two-dimensional FLASH images of the separation of the three gadolinium chelates (see Fig. 11) after degradation of the column performance caused by partial plugging of the inlet frit. Conditions: flow-rate, 3 ml/min, left to right. FL = 90°; T_R = 0.03 s; T_E = 10 ms; SL = 4 mm; matrix size, 256 × 256.

goes from right to left in the Figs. 15–18. Obviously, a small hole and a zone of high permeability has formed against the left wall and the injected band has migrated much faster in this part of the column. In the rest of the column, the packing seems to be quite homogeneous. Like in the former case, the mobile phase velocity seems to be nearly constant outside the perturbed area at the inlet, giving near plug-flow migration of the distorted band (cf. Fig. 7). Horizontal spin echo (Fig. 17) and vertical FLASH images (Fig. 18) of the column inlet regions were taken as in the previous case (Figs. 15 and 16). Their interpretation requires some more information regarding the nature of the NMR signal.

Since the relaxation times T_1 and T_2 are differently influenced by the experimental conditions, namely by the factors which influence the interactions of the protons with their local environment, it is possible to adjust the signal so as to have either a static or a dynamic view of the column. In the former case, the influence of the mobile phase velocity is reduced to a minimum and the image describes the distribution of the concentrations of ^1H, of gadolinium, and of paramagnetic ions. In the latter case, channels where the mobile phase flows appear darker than stagnant pools and some estimate of relative velocities is possible. The comparison of different images permit the recognition of differences in packing density, channel patterns, degree of wetting of the stationary phase, and mobile phase velocity in channels. A crack in the column bed can be visualized because the protons in this channel relax more slowly than those in the small spaces between or inside particles. Accordingly, they appear to be darker.

Figs. 17 and 18 show images which confirm the presence of a crack at the beginning of the packing. The occurrence of the T_2 effect is underlined by arrows in Fig. 17b (frame 5). After a certain migration distance, the complexes dilute and become visible through the T_1 effect (e.g., compare frames 3 and 4, Fig. 15). The band profile results from the combination of very fast migration along the crack and slower, quasi plug-flow migration everywhere else. Fig. 17a illustrates clearly why the presence of a hole at the inlet of a column is so damaging for its efficiency. The hole observed in this case is rather important, however, as seen in Fig. 18 and conclusions regarding the influence of the size of small holes cannot be drawn. Frames 6–9 show its horizontal cross-section. The arrow in frame 6 indicates the beginning of the hole. Another observation to be made in Figs. 17 and 18 is the abundance of black spots at this end of the column compared to the other end (Figs. 7–14). Since the column has been packed by sedimentation, it is expected that the metallic particles, denser than silica fall earlier to the bottom. They are made visible by the considerable reduction that they cause in the relaxation time of the neighbor water protons. Physical examination of the column confirmed, as expected, the presence of particles, some of them metallic or oxides, on the inlet filter and of a hole at the other end, along the column wall.

After replacing the flow distributor, the filter, and the first 1.5 cm of packing and filling the hole, the column was replaced in the scanner and operated with the mobile phase flowing in the

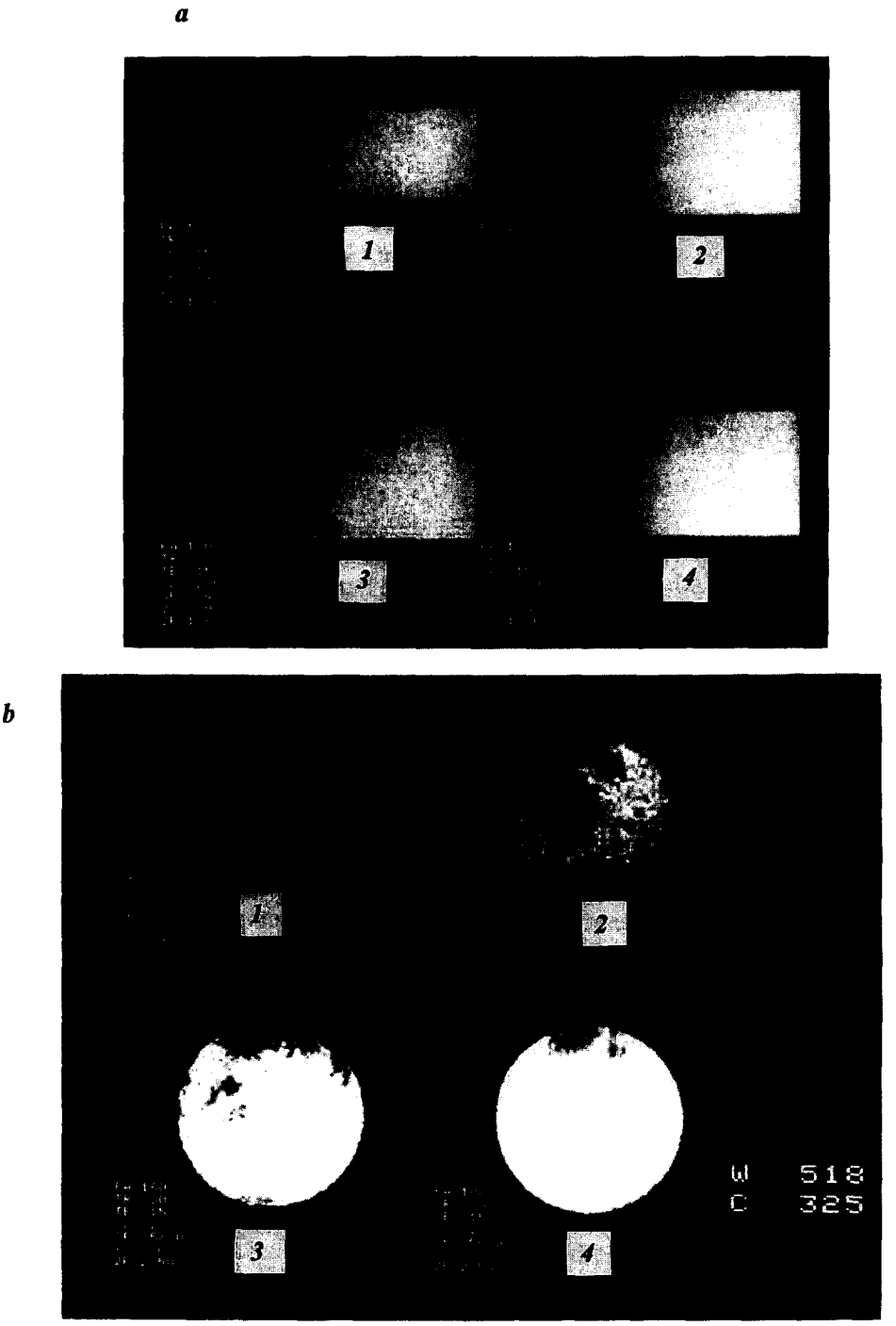

Fig. 14. Three-dimensional spin-echo images of the beginning of the column. (a) Series of parallel slices, 2 mm apart, around the middle of the column. (b) Series of vertical slices, starting from the filter and 2 mm apart.

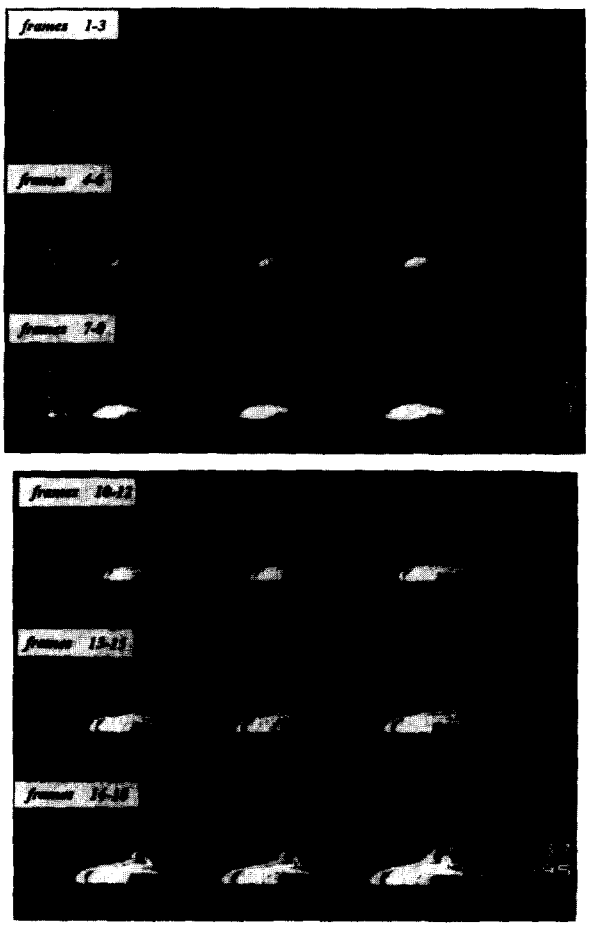

Fig. 15. Two-dimensional FLASH images of the bands of Gd(EGTA), Gd(CDTA) and Gd(DTPA) during their separation. Same NMR conditions as for Fig. 13. Flow-rate, 6 ml/min, right to left.

initial direction. The images of the band profiles obtained (Figs. 19 and 20) show a considerable improvement in the general shape, although the bands are slightly wider and diffuse. The curvature of the three bands in Fig. 19a suggests that either the top of the new packing was not flat, or its density was slightly higher along the wall than in the center. However, there is again near plug-flow migration. In Fig. 20, the bands are nearly flat, showing that the repair has been satisfactory. However, the bands are now more diffuse than in Figs. 7–9, in agreement with the reduced

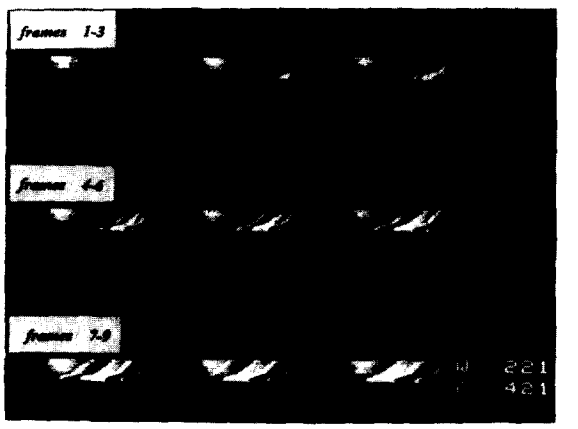

Fig. 16. Two-dimensional FLASH images of the bands of Gd(EGTA), Gd(CDTA) and Gd(DTPA) during their separation. Same as Fig. 15, but extending over longer migration distance. Frames 1 and 2 are frames 6 and 15 in Fig. 15.

column efficiency. The reduced HETP increases from 2.1 to 5.1, suggesting that the new packing is not as regular and homogeneous as the original one.

5. Conclusions

The results described in this work may appear to contradict previous reports in the literature regarding the lack of homogeneity of packed chromatographic columns. We note, however, that, while authors using dry-packing [3–6,10–13] or slurry-packing methods [8,9] find the bed to be radially heterogeneous, with a lower permeability in the center (dry packing, particle size discrimination) or along the wall (slurry packing, probably an effect of the Poiseuille flow profile in the slurry), we find the bed to be extremely homogeneous, with near plug-flow everywhere except in some regions near the column inlet. NMR images show that the reduced HETP in the bed can be as low as 1.0. The column performance is easily degraded, however mainly related to phenomena taking place when the injected band of sample enters the column. Chromatographers have always felt that performing a "correct" injection was a most critical

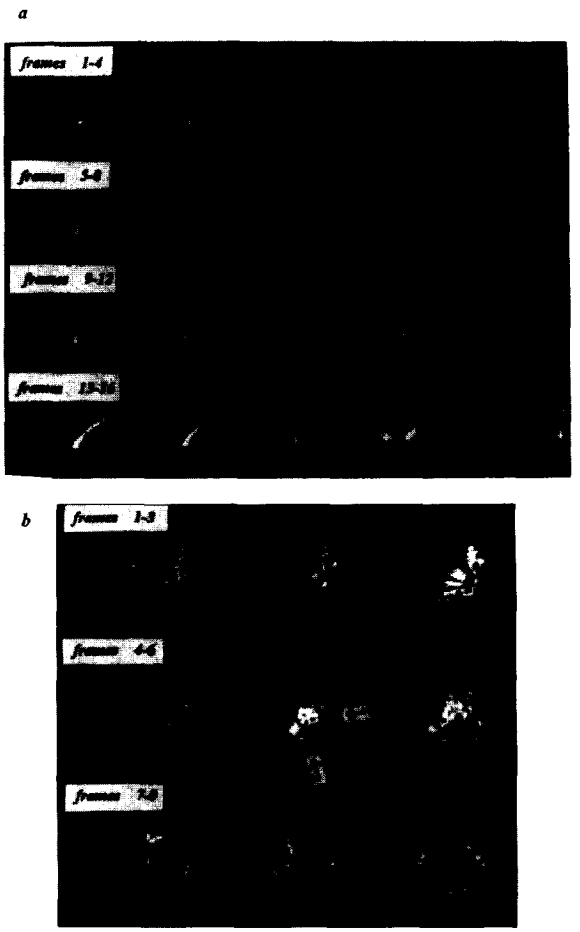

Fig. 17. Three-dimensional FLASH images of the bands of Gd(EDTA) and Gd(DTPA) ca. 2.5 min after injection. FL = 90°; T_R = 0.04 s; T_E = 10 ms; SL = 1 mm; matrix size, 256 × 256. (a) Horizontal slices starting from its middle (frame 1) and going to its top (frame 16), ca. 0.8 mm apart. (b) Vertical slices, starting ca. 12 mm inside the column (frame 1) and going toward the inlet (frame 9).

step in achieving high column efficiency [7] but have always lacked a clear illustration of the difficulties associated with it.

Obstruction of the inlet frit or cracks resulting from uneven consolidation of the bed cause considerable deformation of the band profile, the sample zone moving much faster when entering some parts of the bed than in others. Thus, not filtering the mobile phase before it enters the chromatographic system is dangerous for the column, resulting in performance rapidly ruined. Similarly, the direction of flow in a column should not be reversed. Consolidation of the packing is a slow process, not fully understood. The apparent density of the packing may vary by 10 to 20% depending on the conditions under which it is packed and the procedures used to compress it [63]. The mobile phase flows through the packing, so the pressure gradient, the local velocity and the friction stress applied by the liquid stream to the packing are constant in an homogeneous bed, and this results in an homogeneous contribution to consolidation. Nevertheless, since the bed does not move, there is a static compression pressure applied to the packing, which is equal to the inlet pressure less the friction of the bed along the wall (friction which explains why it is not possible to empty some columns from their packing just by taking off the end frit). This pressure causes uneven consolidation and results in a bed which is denser at the inlet than at the outlet [63]. Reversing the flow direction in the bed causes consolidation to proceed again in the opposite direction and, even in a conventional analytical column, there are no reasons for this consolidation to take place homogeneously. The formation of holes or zones of higher local permeability is quite possible as a result of the collapse of local vaults in the packing.

Finally, our results also confirm that the local separations achieved are often much better than the apparent separations recorded with a bulk detector. As already remarked by Horne et al. [5] and confirmed by Baur et al. [8] and Farkas et al. [9], considerable improvements in the resolution achieved in analytical applications would be obtained if bulk detectors were replaced by local detectors.

Acknowledgement

We thank the Alexander von Humboldt Stiftung (Bonn, Germany) for the Research Award received by G.G.

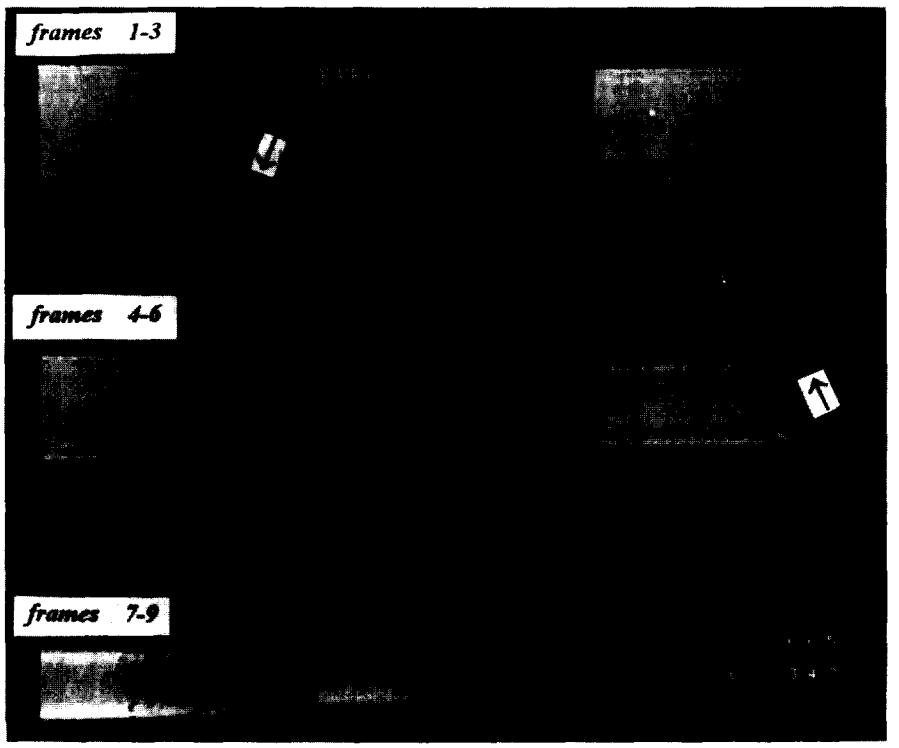

Fig. 18. Three-dimensional spin-echo images of the initial part of the column bed. FL = 90°; T_R = 0.03 s; T_E = 10 ms; SL = 4 mm; matrix size, 256 × 256. The crack which is at the origin of the gross deformation of the band profile is indicated by arrows. In frame 8 it extends over both sides of the column and in frame 9 it occupies the entire section.

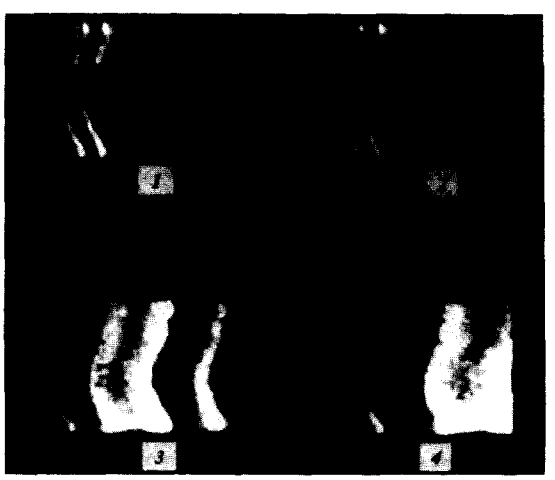

Fig. 19. Two-dimensional FLASH images of the bands of Gd(EGTA), Gd(CDTA) and Gd(DTPA) during their separation on the repaired column. Flow-rate, 6 ml/min, left to right. Same NMR conditions as for Fig. 13.

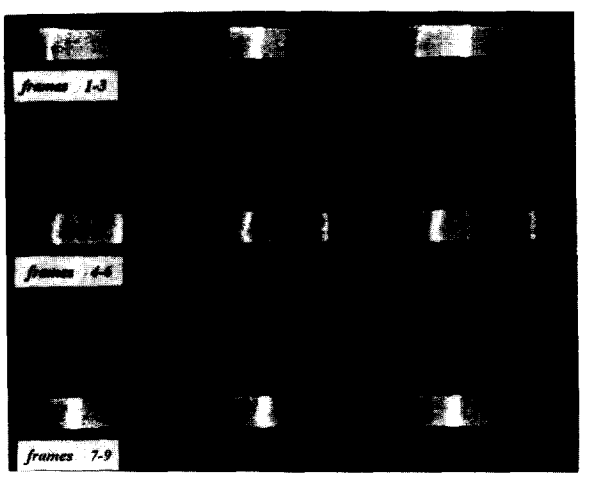

Fig. 20. Two-dimensional FLASH images of the bands of Gd(EDTA) and Gd(DTPA) during their separation on the repaired column. Same experimental conditions as for Fig. 19.

References

[1] J.C. Giddings, *J. Gas Chromatogr.*, 1 (1963) 12.
[2] T. Yun and G. Guiochon, *J. Chromatogr.*, in press.
[3] J.H. Knox and J. Parcher, *Anal. Chem.*, 41 (1969) 1599.
[4] J.H. Knox, G.R. Laird and P.A. Raven, *J. Chromatogr.*, 122 (1976) 129.
[5] D.S. Horne, J.H. Knox and L. McLaren, *Sep. Sci.*, 1 (1966) 531.
[6] C. Eon, *J. Chromatogr.*, 149 (1978) 29.
[7] W.M. Skea, in P.R. Brown and R.A. Hartwick (Editors), *High Performance Liquid Chromatography*, Wiley, New York, 1989, p. 496.
[8] J.E. Baur, E.W. Kristensen and R.M. Wightman, *Anal. Chem.*, 60 (1988) 2338.
[9] T. Farkas, J.Q. Chambers and G. Guiochon, *J. Chromatogr.*, in press.
[10] R.A. Bernard and R.H. Wilhelm, *Chem. Eng. Progr.*, 46 (1950) 233.
[11] C.E. Schwartz and J.M. Smith, *Ind. Eng. Chem.*, 45 (1953) 1209.
[12] F.H. Huyten, W. van Beersum and G.W.A. Rijnders, in R.P.W. Scott (Editor), *Gas Chromatography 1960*, Butterworths, London, 1960, p. 224.
[13] J.C. Giddings and E.N. Fuller, *J. Chromatogr.*, 7 (1962) 255.
[14] T. Yun and G. Guiochon, in preparation.
[15] H. Colin, P. Hilaireau and J. de Tournemire, *LC·GC*, 3 (1990) 40.
[16] H. Colin, in G. Ganetsos and P.E. Barker (Editors), *Preparative and Production Scale Chromatography*, Marcel Dekker, New York, 1993, p. 11.
[17] M.J. Golay and J.G. Atwood, *J. Chromatogr.*, 186 (1979) 353.
[18] M. Sarker and G. Guiochon, *LC·GC*, 12 (1994) 300.
[19] E.B. Byrne and L. Lapidus, *J. Am. Chem. Soc.*, 77 (1955) 6506.
[20] G. Hesse and H. Engelhardt, *J. Chromatogr.*, 21 (1966) 223.
[21] E. Bayer, W. Müller, M. Ilg and K. Albert, *Angew. Chem., Int. Ed. Engl.*, 28 (1989) 1029.
[22] M. Ilg, J. Maier-Rosenkranz, W. Müller, K. Albert, E. Bayer and D. Höpfel, *J. Magn. Reson.*, 96 (1992) 335.
[23] M. Ilg, J. Maier-Rosenkranz, W. Müller. and E. Bayer, *J. Chromatogr.*, 517 (1990) 263.
[24] E. Baumeister, U. Klose, K. Albert, E. Bayer and G. Guiochon, *J. Chromatogr.*, in press.
[25] E. Baumeister, *Dissertation*, Universität Tübingen, Tübingen, 1994.
[26] U. Tallarek, *M.Sc. Dissertation*, Universität Tübingen, Tübingen, 1994.
[27] F.W. Wehrli, D. Shaw and J.B. Kneeland (Editors), *Biomedical Magnetic Resonance Imaging*, VCH, New York, 1988.
[28] R.A. Komoroski, *Anal. Chem.*, 65 (1993) 1068A.
[29] H.V. Carr and E.M. Purcell, *Phys. Rev.*, 94 (1954) 630.
[30] R. Bradford, C. Clay and E. Strick, *Phys. Rev.*, 84 (1954) 157.
[31] R. Damadian, *Science*, 171 (1971) 1151.
[32] P.C. Lauterbur, *Nature*, 242 (1973) 190.
[33] P. Mansfield and P.K. Grannell, *J. Phys.*, C6 (1973) 422.
[34] P. Mansfield and P.G. Morris, in *Advances in Magnetic Resonance*, Academic Press, New York, 1982, Ch. 3.
[35] W. Kuhn, *Angew. Chem., Int. Ed. Engl.*, 29 (1990) 1.
[36] G.D. Fullerton, *Magn. Reson. Imag.*, 1 (1982) 39.
[37] P.T. Callaghan, *Principles of Nuclear Magnetic Resonance Microscopy*, Clarendon, New York, 1991, Ch. 3.
[38] F.A. Bovey, *Nuclear Magnetic Resonance Spectroscopy*, Academic Press, New York, 1988, p. 492.
[39] P.T. Callaghan, *Principles of Nuclear Magnetic Resonance Microscopy*, Clarendon, New York, 1991, p. 5.
[40] P. Mansfield and P.K. Grannell, *Phys. Rev.*, 12 (1975) 3618.
[41] P. Mansfield, *J. Phys.*, E21 (1988) 18.
[42] A. Kumar, D. Welti and R.R. Ernst, *J. Magn. Reson.*, 18 (1975) 69.
[43] W.A. Edelstein, J.M.S. Hutchison, G. Johnson, T.W. Redpath and L.M. Eastwood, *Phys. Med. Biol.*, 25 (1980) 751.
[44] G. Johnson, J.M.S. Hutchison, T.W. Redpath, L.M. Eastwood, *J. Magn. Reson.*, 54 (1983) 374.
[45] E. Baumeister, K. Albert and E. Bayer, in preparation.
[46] Ch. Kittel, *Introduction to Solid State Physics*, Wiley, New York, 1986, Ch. 14.
[47] R.B. Lauffer, *Chem. Rev.*, 87 (1987) 901.
[48] D.G. Gadian, J.A. Payne, D.J. Bryant, I.R. Young, D.H. Carr and G.M. Bydder, *J. Comput. Assist. Tomogr.*, 9 (1985) 242.
[49] S.H. Koenig and R.D. Brown, *Magn. Reson. Med.*, 1 (1984) 478.
[50] S.H. Koenig, C. Baglin, R.D. Brown and C.F. Brewer, *Magn. Reson. Med.*, 1 (1984) 496.
[51] C.D. Barry, A.C.T. North, J.A. Glasel, R.J.P. Williams and A.V. Xavier, *Nature*, 232 (1971) 236.
[52] W. Grodd and R.C. Brasch, *Fortschr. Röntgenstr.*, 145 (1986) 130.
[53] P.T. Callaghan, *Principles of Nuclear Magnetic Resonance Microscopy*, Clarendon, New York, 1991, Ch. 5.3.
[54] G. Sosnovsky and N.U.M. Rao, *Eur. J. Med. Chem.*, 23 (1988) 517.
[55] H.J. Weinmann, R.C. Brasch, W.R. Press and G.E. Wesley, *Am. J. Roentgenol.*, 142 (1984) 619.
[56] M.M. Vora, S. Wukovnig, R.D. Finn, A.M. Emran, T.E. Boothe and P.J. Kotari, *J. Chromatogr.*, 369 (1986) 187.
[57] T. Moeller and L.C. Thompson, *J. Inorg. Nucl. Chem.*, 24 (1962) 499.
[58] E. Merciny and J. Fuger, *Anal. Chim. Acta*, 160 (1984) 87.
[59] R.S. Kolat and J.E. Powell, *Inorg. Chem.*, 1 (1962) 485.
[60] D. Matthaei, J. Frahm and A. Haase, *Magn. Reson. Imag.*, 4 (1986) 381.
[61] A. Haase, J. Frahm, D. Matthaei, W. Hänicke and K.-D. Merboldt, *J. Magn. Reson.*, 67 (1986) 258.
[62] V.M. Runge (Editor), *Enhanced Magnetic Resonance Imaging*, Mosby, St. Louis, MO, 1989, Ch. 5.
[63] G. Guiochon and M. Sarker, in preparation.